Materials Science & Engineering A 839 (2022) 142845

Contents lists available at ScienceDirect

Materials Science & Engineering A

journal homepage: www.elsevier.com/locate/msea

Influence of chemical composition and thermomechanical treatment of low-carbon steels on the microstructure and mechanical properties of their laser welded joints

A.I. Gordienko [a,*], A.G. Malikov [b], M.N. Volochaev [c,d], A.D. Panyukhina [e]

[a] Institute of Strength Physics and Materials Science of Siberian Branch Russian Academy of Sciences, 2/4, Pr. Akademicheskii, Tomsk, 634055, Russia
[b] Khristianovich Institute of Theoretical and Applied Mechanics of the Siberian Branch of the Russian Academy of Sciences, 4/1, Institutskaya str., Novosibirsk, 630090, Russia
[c] Kirensky Institute of Physics of the Siberian Branch of the Russian Academy of Sciences (SB RAS), Akademgorodok 50, bld. 38, Krasnoyarsk, 660036, Russia
[d] Reshetnev Siberian State University of Science and Technology, 31, Pr. Krasnoyarsk worker, Krasnoyarsk, 660037, Russia
[e] Tomsk Polytechnic University, 30, Lenin Avenue, Tomsk, 634050, Russia

ARTICLE INFO

Keywords:
Low-carbon steels
Laser welding
Cross-helical rolling
Weld metal
Microstructure
Microhardness

ABSTRACT

The paper reports microstructures (revealed by transmission electron microscopy) in various zones of laser welds of the X70 and X80 low-carbon steels with different initial microstructures, as well as chemical and phase compositions. In the X70 steels with 0.13% C, the microstructure refinement has been achieved through helical rolling at temperatures of 920 °C and 850 °C (designated as X70-920 and X70-850, respectively). For all studied cases, both initial steel microstructures and phase compositions have determined the formation of different microstructures with various microhardness levels in the weld metal and heat-affected zones. For the X70-850 steel with a more dispersed and homogeneous microstructure (d_F = 3.3 μm), a lower microhardness level of 340 HV has been observed in the weld metal, compared with the X70-920 one (d_F = 5.5 μm, 370 HV). The reason has been the formation of both bainite and martensite laths in the X70-850 weld metal, while only lath and lamellar martensite has formed in the X70-920 one. For the X80 steel (0.55% C), lowering the carbon content and additional microalloying with chromium, molybdenum and nickel have enabled to decrease the microhardness level down to 295 HV in the weld metal due to the degenerate upper bainite formation and the carbon level reduction in martensite. The dispersed and homogeneous initial microstructures of the X70-850 and X80 steels has provided the formation of granular ferrite-bainite microstructures in the intercritical heat-affected zone. They have possessed a lower proportion of residual austenite regions and small sizes of twinned martensite areas. The welded X80 steel specimen has been characterized by higher ductile properties compared to both X70 ones.

1. Introduction

Low-carbon low-alloy steels are widely used in the automotive and construction industries, particularly in both overland and submarine pipelines for oil and gas transportation. Typically, a variety of arc welding methods are implemented to join parts of such steels into structures [1–3]. However, these processes are characterized by great heat input levels, which causes the formation of wide heat-affected zones (HAZ) with uneven resistance to plastic strains and fracture. In order to reduce the heat input levels, advanced joining technologies are being developed, such as laser welding [4]. Its deployment results in a number of advantages, such as high welding speed and efficiency, narrow HAZ and low distortions, etc. [5–8]. However, this process leads to increased hardness [5–8] and brittleness [9] of laser welds, which significantly inhibits its implementation. Therefore, an issue of improving ductility of the joints is urgent.

In laser welding, both heating and cooling conditions determine the microstructure in formed joints. In this regard, the influence of its parameters (power and welding speed) on the microhardness level in laser welds of low-carbon steels has been reported in Refs. [7,8,10]. It has been shown that it is impossible to avoid the formation of quenched martensitic microstructures in their weld metal (WM) [7,10]. With a decrease in welding speed, only lengths of laths and distances between them in martensite increase, while the hardness level remains high.

* Corresponding author.
E-mail address: mirantil@sibmail.com (A.I. Gordienko).

https://doi.org/10.1016/j.msea.2022.142845
Received 30 September 2021; Received in revised form 15 February 2022; Accepted 15 February 2022
Available online 18 February 2022

An important role in the weld microstructure formation is played by the chemical composition of the steels. Varying carbon contents and microalloying with various elements changes both points of their phase transformations and the microstructure types, as well as volume fractions and sizes of second phase particles. It has been shown in Refs. [11–13] that a decrease in the carbon content promotes an increase in the beginning points of the bainite transformation and the granular bainite formation. In addition, the carbon proportion in the martensite-austenite (M-A) constituent decreases, which contributes to improvement of their ductility. Also, microalloying of the steels with chromium, molybdenum, and nickel causes lowering the beginning points of the bainite transformation and an expansion of the range of its development [13–15].

Since the processes of phase transformations upon heating and decomposition of supercooled austenite begin at grain boundaries, their kinetics and the weld microstructures depend on the morphology and grain sizes of prior austenite [16]. It has been shown in Refs. [17–22] that a decrease in dimensions of austenite grains results in reducing the beginning points of the martensite transformation, as well as sizes of both martensite packets and blocks [20]. The authors of [17,18] have noted that widths of martensite laths do not depend on dimensions of austenite grains, but their lengths rise with enlargement of austenite grains.

An increase in the dispersion of austenite grains contributes to enhancing of the starting (Bs) and final (Bf) points of the bainite transformation [23,24]. Eroglu M. et al. [25] have investigated the effect of grain sizes on the microstructure and fracture toughness of the intercritical (IC) HAZ of the low-carbon steels. It has been shown that the initial small grain sizes contribute to the formation of ductile phases characterized by lower microhardness and higher fracture toughness. In contrast, coarse initial grains result in the formation of brittle phases such as martensite and ferrite, as well as lower fracture toughness of the steels.

The initial phase composition and the carbon distribution uniformity in the steels affect the formation of the weld microstructure. It has been revealed in Ref. [26] that a great proportion of the M-A constituent regions is formed in the microstructure in the case of an inhomogeneous carbon distribution upon heating in the (A_{c1}–A_{c3}) intercritical interval and subsequent rapid cooling. Akselsen O.M. et al. have shown [27] that the IC HAZ microstructure depends on the initial pearlite volume fractions and sizes. Large dimensions of the pearlite regions result in the formation of a high volume fraction of the M-A constituent and twinned martensite areas in the IC HAZ, causing embrittlement of the welds. Finally, the dispersed and homogeneous microstructure of the base metal without pronounced ferrite-pearlite banding contributes to a decrease in the HAZ hardness [28].

It should be noted that patterns of the steel microstructure formation have been studied either after thermomechanical treatment (which does not quite reflect the real conditions of the processes occurring upon welding), or during investigations of the coarse-grained HAZ (since it is believed that this region is the most critical). However, the highest hardness level is often observed in the WM of laser welds [28], so an important task is to understand ways to reduce its brittleness. In this regard, the aim of this paper is to report the effect of both chemical and phase compositions, as well as the initial microstructure of the X70 and X80 low-carbon steels on the patterns of the microstructure formation and mechanical properties of their laser welded joints.

After laser welding, cooling rates determine by thicknesses of the joined plates (from 1.2 up to 2.0 mm in Refs. [5,7–9]). In these cases, they did not reflect actual dimensions of any products under operating conditions. However, the obtained results could be useful for the correct choice of materials for thicker parts to be welded by identifying factors that reduce the brittleness of those for thinner ones.

2. Materials and methods

2.1. Materials

Two low-carbon low-alloyed steels of the X70 and X80 grades were investigated, which differed in the contents of carbon and alloying elements (Table 1). The X80 steel contained less carbon but was additionally microalloyed with chromium, molybdenum and nickel.

The initial microstructure of the X70 steel was changed by helical rolling at temperatures of 920 °C and 850 °C (designated as X70-920 and X70-850, respectively). In both cases, six rolling passes were carried out, followed by continuous air cooling. A diameter of the initial X70 steel bars was 40 mm. After six helical rolling passes, it was reduced down to ≈18 mm. The total reduction degree (φ) was calculated according to the formula $\varphi = \sum \ln(F_{i-1}/F_i)$, where F_{i-1} and F_i were the initial and final cross-sectional areas of the bars (about 1.6).

It was shown in Ref. [29] that the steel microstructure was refined with a decrease in the rolling temperature (Fig. 1a and b). Also, the pearlite volume fraction decreased down to 8% (Table 2), as well as the VC, Fe_3C, Fe_2C carbides were found in the microstructure [29].

The investigated X80 steel (designated as X80 below) was received after controlled longitudinal rolling finished in the (γ+α)-region, followed by rapid cooling down to the bainite transformation temperatures and final cooling in air. As a result, a predominantly ferrite-bainite microstructure had formed with small troostit areas (Fig. 1, c; Table 2). The microstructure contained fine Nb_2C carbides with sizes of 5–10 nm, the Fe_3C, Fe_2C, and Mn_7C_3 ones, as well as the FeAl intermetallic compounds.

2.2. Welding conditions

Since the welded plate thickness was 1.2 mm in the previous studies of the authors [9,28], similar ones were joined in this research for comparison. Rectangular steel sheets with dimensions of 90 × 18 × 1.2 mm (for the X70 steel) and 90 × 30 × 1.2 mm (for the X80 one) were cut from rods and plates. Keyhole single-pass welding was carried out in the direction perpendicular to the workpiece axis using the 'Siberia-1' automatic setup [30,31], including a continuous CO_2 laser with a maximum power of 8 kW. Joints were obtained at a power of 1.2 kW and welding speed of 1 m/min. A laser beam was focused 2 mm underneath the plate surfaces. Both weld zones and roots were shielded with an inert gas (helium).

2.3. Microstructural studies

In the laser welds, microstructures were examined using a 'Zeiss Axiovert 25' optical microscope (OM), a 'LEO EVO 50' scanning electron microscope (SEM), and an 'HT-7700' transmission electron microscope (TEM). Etching of cross-sections for both metallographic and SEM studies was carried out in a 3% HNO_3 alcohol solution. In order to locally study the microstructures in the weld areas, a 'FIB2100' focused ion beam system was used to cut out foils from both WM and HAZ. The average grain sizes were determined using the OM, SEM, and TEM images by the method of random cutting lines. To determine the area fraction of retained austenite, the counting point method was applied with a point grid that was superimposed on the TEM images.

2.4. Mechanical tests

Vickers microhardness values were determined along the longitudinal weld axis by a 'PMT-3' setup at a load of 100 g. At least five measurements were performed at one test point. Uniaxial static tensile tests were carried out using a 'Polyani' facility with automatic recording of loading curves at room temperature and a load rate of ~2 μm/s. 'Dog-bone' samples were cut by electric discharge machining. Their thinned parts were 15 × 3 × 1.2 mm. The welds were in the center of the

Table 1
Chemical composition of the studied steels (wt. %).

	Fe	C	Mn	Si	Nb	V	Ti	Mo+Ni + Cr	Cu	Al	P	S
X70	97.38	0.13	1.6	0.40	0.04	0.05	0.05	–	0.30	0.03	0.013	0.010
X80	97.6	0.055	1.59	0.07	0.05	0.05	0.02	0.397	0.12	0.03	0.006	0.004

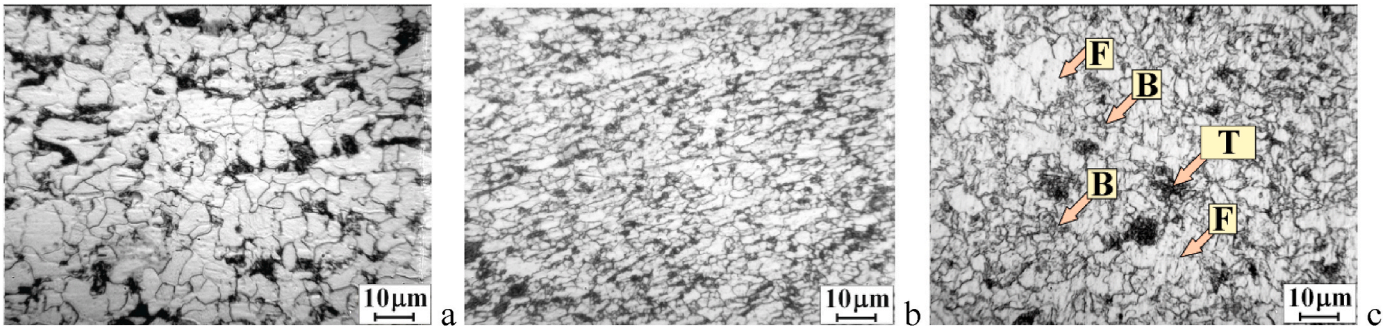

Fig. 1. The microstructures of the X70-920 (a), X70-850 (b) and X80 (c) steels: F is ferrite, B is bainite, T is troostite.

Table 2
The microstructural characteristics of the studied steels.

	Phase composition[a]	d_F, μm	HV_{100}	Carbides and intermetallic compounds
X70-920	F+16%B+11%P	5.5	185 to 200	VC, Fe_3C, Fe_2C
X70-850	F+17%B +8%P	3.3		
X80	F+40%B+6%T	4.0	210	Nb_2C, Fe_3C, Fe_2C, Mn_7C_3, FeAl

[a] F is ferrite; B is bainite; P is perlite; T is troostite; d_F is the average size of ferrite grains.

samples.

3. Results

3.1. The macrostructures and microhardness in the welds

Macrostructures of the laser welded joints of the steels of different initial conditions were similar in general (Fig. 2). Their widths did not exceed 2.0–2.5 mm; both WM and HAZ were observed. So far as heating and cooling rates had been higher upon laser welding than those in conventional arc welding procedures, the HAZ was narrow and its typical characteristic regions (for example, a zone of recrystallized grains) were not revealed inside (Fig. 2).

In the welds, microhardness levels increased significantly in comparison with those in the base metals (Fig. 2, d), but in different ways for various initial steel conditions. The greatest increase in the microhardness values up to 370 HV was found in the X70-920 WM. As the distance from the WM to the base metal reduced, the microhardness level decreased. For the same steel after rolling from 850 °C (X70-850), the microhardness values were below 340 HV in the WM, while they reduced down to 295 HV in the X80 WM. The microhardness values in the HAZ gradually decrease as they approach the base material (BM). In contrast to the X70-920 and X70-850 steels, a lower microhardness level was observed in the HAZ region of the X80 steel.

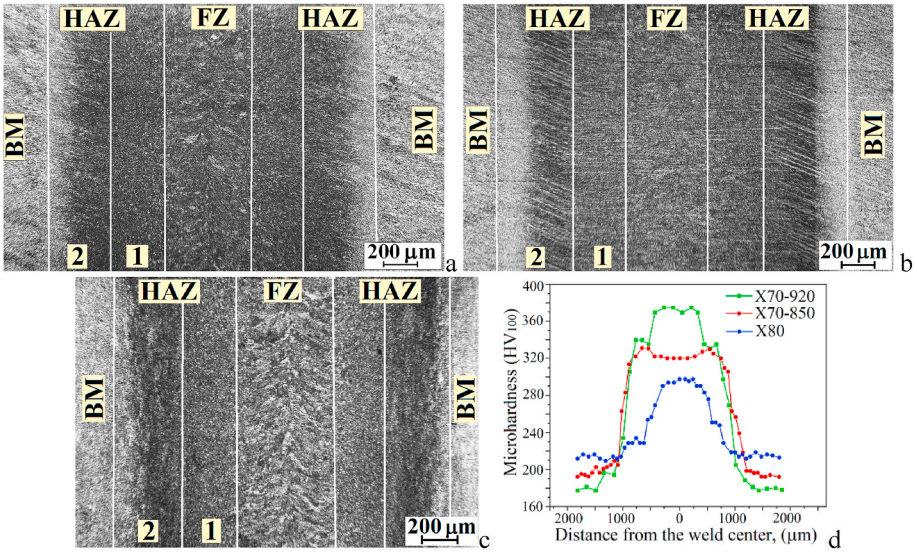

Fig. 2. The macrostructures of the welded joints of the X70-920 (a), X70-850 (b), and X80 (c) steels, as well as their microhardness distributions (d): 1 – fine-grained HAZ; 2– intercritical HAZ.

3.2. The microstructural studies in the weld metal zones

Since the WM microhardness differed significantly, fine structures in these regions were studied in detail. The WM widths were in the range of 500–570 μm for all initial steel conditions. After laser welding, rapid solidification of weld pools had occurred from their edges towards the centers. Therefore, dendritic microstructures had formed in the WM (Fig. 2, a). In the X70-920 WM, lath martensite areas were observed (Fig. 3, a, indicated by a yellow arrow) in addition to plate-type martensite, represented by long and wide needles (Fig. 3, a, indicated by a white arrow).

The lath widths varied in the range from 150 up to 900 nm, while the largest needles reached 1.8 μm. TEM images show thin parallel laths characteristic of packed lath martensite (Fig. 3, c). In wider martensite laths, the Fe_3C carbides were found at an angle of 70° to the lath axis (Fig. 3, d).

In the X70-850 WM, the dendritic microstructure was less pronounced (Fig. 2, b). Martensite laths 130–700 nm wide, bainite laths with fine inclusions inside, and small granular bainite areas were observed in SEM-images (Fig. 4a and b).

In the X80 WM, dendritic elongated regions were also found (Fig. 2, c). However, its microstructure was different compared to the X70 WM. In the X80 WM, both martensite and bainite areas were observed (Fig. 4c and d). According to the results of the TEM studies, widths of martensite laths were from 80 up to 450 nm (Fig. 5, a). Between them, residual austenite regions about 50 nm thick with a volume fraction of 4% were present (Fig. 5b and c).

In the X80 WM, bainite packets were misoriented relative to each other and laths 350–440 nm wide were characterized by discontinuity (Fig. 4c and d and Fig. 5, d). Residual austenite regions were found between bainite laths (Fig. 5, e–f). This microstructure was characteristic of the degenerate upper bainite. The microdiffraction patterns showed reflections of Fe_3C carbides (Fig. 5, e). The dark-field images showed that dispersed Fe_3C carbides were distributed in the bainite matrix (Fig. 5, g–h).

3.3. The microstructural studies in the heat-affected zones

It was shown based on the results of the SEM studies that all investigated steels were characterized by fine-grained (FG) and IC HAZs (Fig. 2, a-c; Fig. 6, as an example of the X70-920 steel). In FG HAZ with dimensions of about 300 μm, the bainite-martensite microstructures had formed (Fig. 6, a–b), varying in packet sizes associated with different heating temperatures of these regions. The closer the region was to the weld metal, the coarser the microstructure was (Fig. 6, a). However, the greatest variations in the microstructures were observed in the IC HAZs. In the X70-920 IC HAZ, the microstructure was coarse-grained and banded (Fig. 6, c), while it was fine and more uniform in the X70-850 and X80 ones (Fig. 7). This was due to the fact that the phase transformations had occurred in the steels upon heating in the IC temperature range and their initial states played a role in the HAZ microstructure formation. Therefore, the detailed TEM studies of the IC HAZ microstructures were performed (Fig. 8).

It was shown that the ferrite-bainite microstructures had formed in the IC HAZ of all steels. In the X70-920 IC HAZ, ferrite grains were larger and bainite possessed a predominantly lath morphology (Fig. 8, a). It should be noted that the degenerate upper bainite with lath thicknesses of 50–200 nm and a small fraction of granular bainite (Fig. 8, b) were also found by the authors of [28] in a similar case. At the boundaries of the bainite regions, there was the M-A constituent of both slender and massive shapes (in the form of retained austenite (Fig. 8, c) and twinned martensite, respectively). Sizes of the retained austenite regions reached 40 × 400 nm, while its proportions were up to 9%, estimated with respect to the specific bainite regions under consideration, but not the entire HAZ. Dimensions of the twinned martensite areas were about 700 × 1600 nm.

In contrast, granular bainite areas 0.5–1.5 μm in size prevailed in the X70-850 IC HAZ (Fig. 8, d). At their boundaries, residual austenite regions 90–200 nm long and 10–30 nm wide were observed (Fig. 9, a–c). In addition, degenerate upper bainite areas were found. At the boundaries of its laths, residual austenite regions up to 400–500 nm in length with a volume fraction of 7% were present (Fig. 9, d). Also, massive-shaped twinned martensite areas were found, which ranged in their sizes from (10–30) × 200 nm up to (40–70) × 600 nm (Fig. 9, e–f). The microdiffraction patterns showed reflections of Fe_3C carbides (Fig. 9, b).

In the X80 IC HAZ, the ferrite-bainite microstructure of predominantly granular morphology had formed (Fig. 8, e; Fig. 10, a). At the granular bainite boundaries, retained austenite interlayers were observed (Fig. 10, c–d) with thicknesses of 20–70 nm and lengths of 120–800 nm. The retained austenite volume fraction was 4%. Along

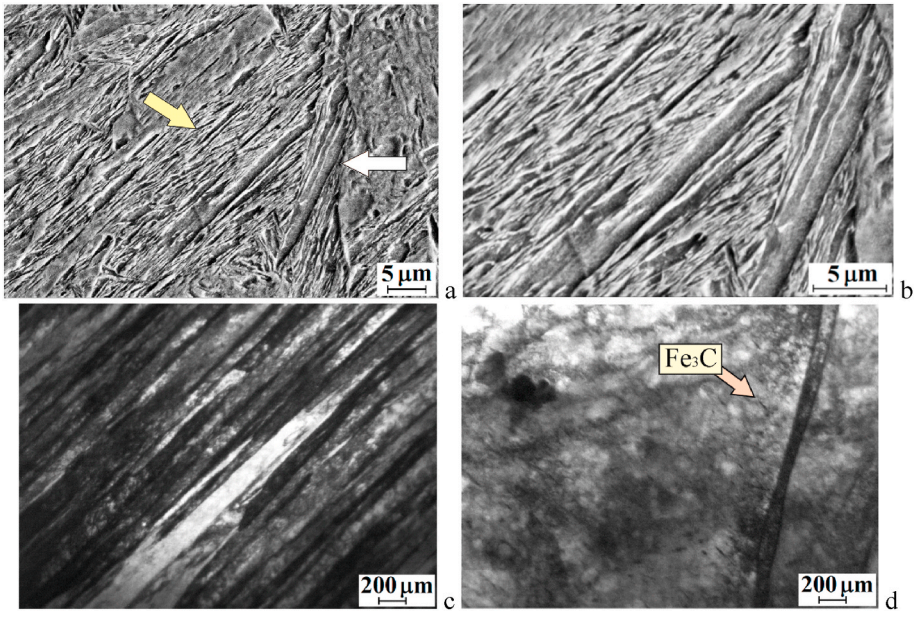

Fig. 3. The SEM (a–b) and TEM (c–d) images of the microstructures in the X70-920 WM: lath martensite and plate-type martensite areas were indicated by a yellow and white arrows, respectively. (For interpretation of the references to colour in this figure legend, the reader is referred to the Web version of this article.)

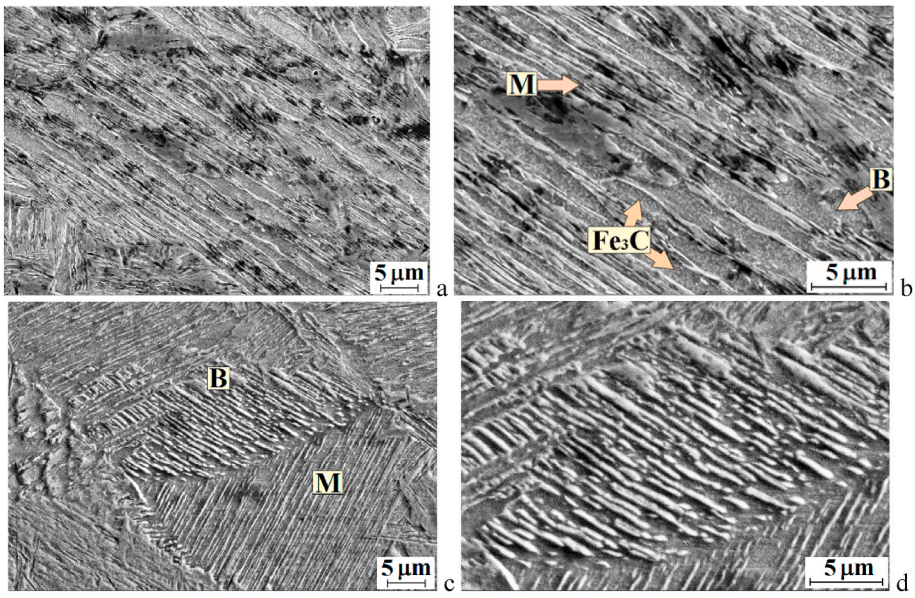

Fig. 4. The SEM images of the WM microstructures in the X70-850 (a and b) and X80 (c and d) steels: M is martensite, B is bainite.

with granular bainite, there was a small proportion of lath bainite. In addition, twinned martensite areas approximately (80–200) × 600 nm in sizes were found (Fig. 10, e-f). The microdiffraction patterns showed reflections of Nb_2C, Fe_3C Fe_2C carbides (Fig. 10, b).

Comparative characteristics of the IC HAZ microstructural components are given in Table 3 for all investigated steels. In should be noted that the X70-920 IC HAZ was distinguished by the degenerate upper bainite microstructure with smaller retained austenite areas (but their greater proportion) and twinned martensite large zones. In both X70-850 and X80 IC HAZs, mainly bainite of granular morphology had formed with a lower proportion of retained austenite and smaller sizes of twinned martensite.

3.4. Tensile tests

The results of the tensile tests showed that the yield points (YS) of both X70-920 and X70-850 welded samples increased by 9–16%, while it was at the base metal level for the X80 one (Table 4). The ultimate tensile strength (UTS) values of the X70-920 and X70-850 welded samples decreased insignificantly, but elongation reduced by about 25%. The strength characteristics of the X80 welded sample remained at the base metal level, while elongation reduced by 11%. All welded samples fractured through the base metals that confirmed the high strengths of the joints.

the same conditions. This fact indicated the possibility of partial controlling of hardness levels in laser welds by changing initial microstructures of base metals.

The results of the TEM studies proved that the reduced hardness values in the X70-850 WM was associated with the lath bainite microstructure formation with lower residual stresses (along with lath martensite), while lath and lamellar martensite was observed in the X70-920 WM. In the X70-850 WM, the bainite formation could be associated with a change in the austenization kinetics upon heating and the subsequent γ→α transformation upon cooling [32]. The initial X70-850 steel condition was distinguished by the more dispersed microstructure ($d_F \approx 3.3$ μm) and the uniform distribution of the microstructural components, in comparison with those of the X70-920 one ($d_F \approx 5.5$ μm). In the case of initial small ferrite grains, the density of austenite nucleation points had increased upon heating [17]. This determined the formation of more dispersed austenite in the X70-850 steel. As shown earlier in Refs. [17–19], the starting martensite transformation point (Ms) decreased in microstructures with small grain sizes. At the same time, the Ms level was sensitive even to small changes in grain dimensions in the case of dispersed microstructures (with a decrease in the austenite grain sizes from 4.7 down to 2.6, the Ms point reduced from 375 down to 361 °C [19]). To confirm this fact, the theoretical Ms levels, calculated according to formula (1) [21,33], were 330 and 318 °C for the X70-920 and X70-850 steel, respectively.

$$Ms = [718.3 - 291X_C - 24X_{Mn} - 1.8X_{Si} - 5.6X_{Cr} - 18.4X_{Ni} + 3.5X_{Mo}] - 7.22^{-1}\left\{\left[\sqrt{\left(195X_{Mn}^{0.5}\right)^2 + \left(140X_{Si}^{0.5}\right)^2 + \left(170X_{Cr}^{0.5}\right)^2 + \left(5X_{Ni}^{0.5}\right)^2 + \left(205X_{Mo}^{0.5}\right)^2} + 670X_C^{0.5}\right] + \left[350D_\gamma^{-0.5}\right] + \left[370exp\left(-6D_\gamma D_C^{-1}\right)\right] + 1015\right\} \quad (1)$$

4. Discussion

As noted above, the main challenge of laser welding of the low-carbon steels was increased hardness in the weld zones due to the formation of quenched microstructures during ultrafast cooling. The research results showed that the WM microhardness levels were different (370 and 340 HV) for the same steel with various initial microstructures (X70-920 and X70-850, respectively) after welding under

It was noted in Ref. [13] that the supercooled austenite stability decreased in fine-grained austenite, which resulted in a shift of the austenite decomposition interval to higher temperatures, as well as an increase in both Bs and Bf points in addition to an expansion of the bainite transformation interval. This explained the lath bainite formation in the X70-850 WM.

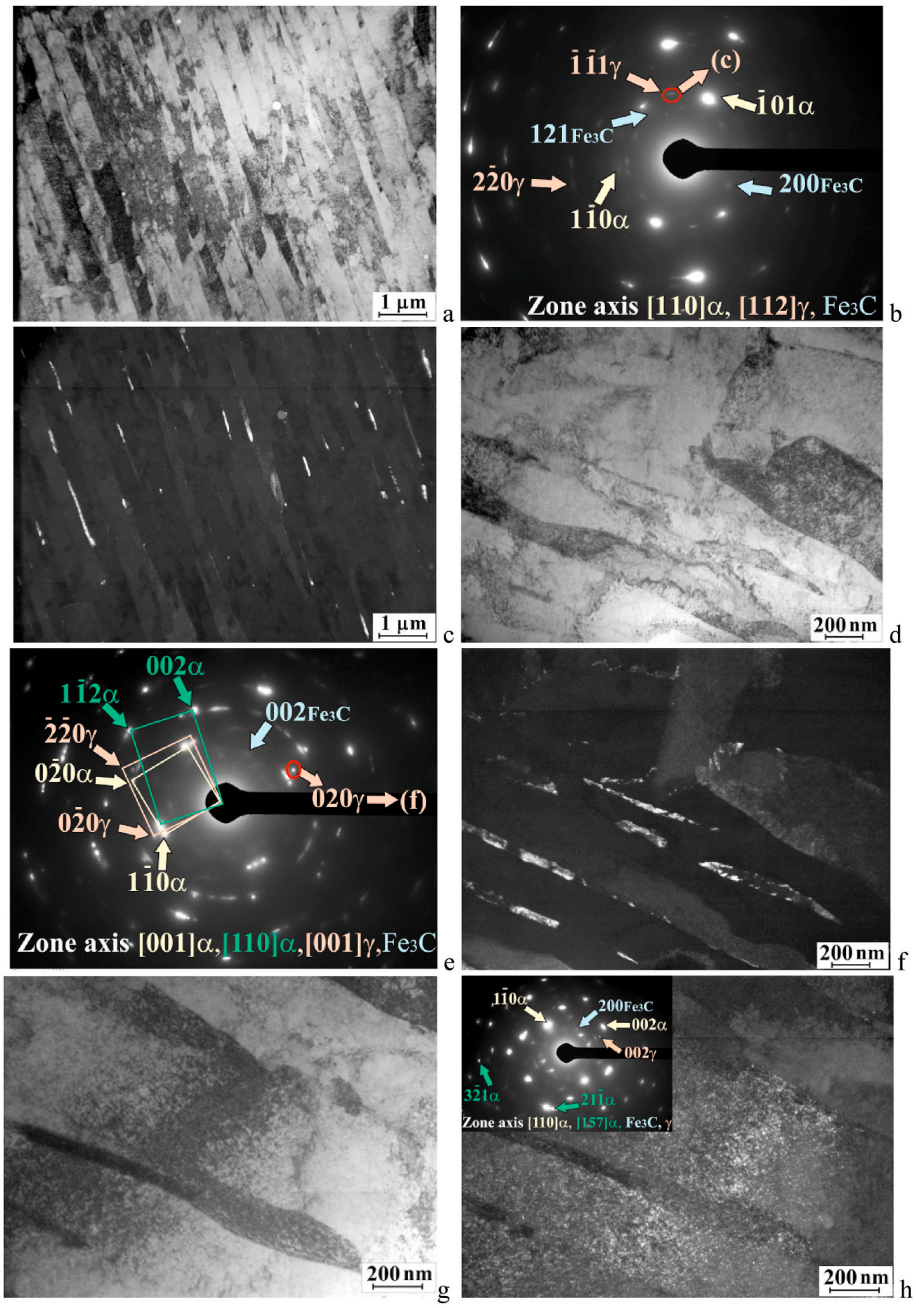

Fig. 5. The TEM-images of the X80 WM microstructure: bright-field image in the martensite region (a), microdiffraction pattern, arrows indicate reflexes of the [111]α, [112]γ, [114]γ zones (b); dark-field image in the $\bar{1}\bar{1}1$ γ reflex (c); bright-field image in the bainite region (d, g); microdiffraction pattern (e); dark-field image in the 020γ reflex (f); dark-field image in the 200 Fe_3C reflex (h).

For the X80 steel, reducing the carbon content, additional microalloying with chromium, molybdenum and nickel, as well as the formation of the complex carbides (Table 2) decreased the tendency for austenite grains to grow upon heating. Also, the X80 steel had the greater bainite proportion in the initial microstructure (Table 2). It was shown in Ref. [26] that the A_{c1} critical point was higher and the austenite transformation occurred at greater temperatures in steels with the bainite microstructure upon heating. Therefore, the transformation range shifted to higher temperatures. This delayed the subsequent recrystallization and growth of austenite grains. As noted by the authors of [34], hardenability of steels increased with coarsening of their grains.

In addition, the decreased carbon content affected the supercooled austenite decomposition, contributing to an increase in the A_3, Bs, and Bf critical transformation points [13] and a decrease in the Ms level [35]. The influence of each alloying element could result in the opposite effect on the phase transformation temperatures and depended on the cooling conditions. Thus, alloying with molybdenum accelerated the austenite-to-ferrite transformation. However, it was found in Ref. [36] that its effect was opposite upon rapid cooling and it increased the austenite stability as well. As a result of the synergistic microalloying effect, chromium, molybdenum and nickel decreased the Bs point [12, 13] but expanded the bainite transformation range due to the reduced Bf level [13]. This determined the bainite microstructure formation in the X80 WM. Also, the carbon content was fewer in martensite of the X80 steel and its microhardness was lower as a result. In the X80 WM, it was only 295 HV that met requirements the DNV-OS-F101 standard [37], according to which it had to be below 300 HV.

Similar dependences were observed when studying the IC HAZ

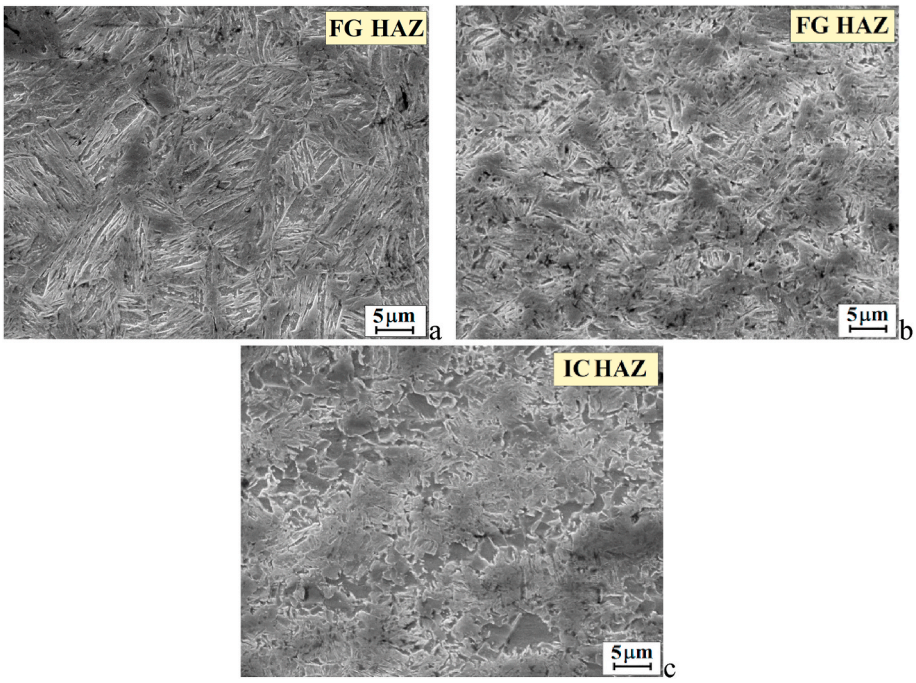

Fig. 6. The SEM images of the HAZ in the X70-920 steel [28].

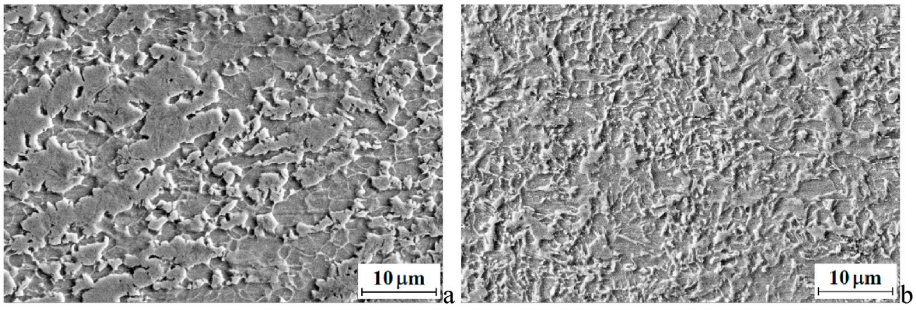

Fig. 7. The SEM-images of the IC HAZ microstructures in the X70-850 (a) and X80 (b) steels.

microstructures. The TEM results confirmed the presence of the relatively higher volume fraction of the low-temperature phase transformation products (lath bainite) in the X70-920 IC HAZ (Fig. 8, a). In both X70-850 and X80 IC HAZs, the granular bainite formation was explained by the increase in the Bs and Bf critical points of the bainite transformation due to the microstructure refinement (X70-850 steel) and the chemical composition changes (the X80 steel). In the X70-920 steel, the microstructural heterogeneity was expressed (Fig. 1, a) and coarse pearlite grains were present. Considering the rapid heating upon laser welding, the formed austenite had been inhomogeneous in its chemical composition. Upon cooling, the weld metal microstructure had inherited the austenite inhomogeneities [38]. This caused the formation of areas with the higher carbon contents. As a result, the X70-920 IC HAZ was characterized by the greatest proportion of retained austenite areas and extensive twinned martensite regions (Table 3). Despite the different microstructures in the IC HAZ of the X70-920 and X70-850 steels, their microhardness levels were high and roughly comparable (Fig. 2, d). This could be due to the dispersion of the microstructures and insufficient locality of the Vickers microhardness measurement method. At the load of 100 g, the imprint diagonal size was ≈20–25 μm. In other words, one imprint located at both bainite and ferrite regions, so the microstructures values were averaged. However, the presence of the M-A component and twinned martensite had to be considered because they could have the greatest effect in impact bending tests.

In contrast to the X70-920 and X70-850 steels, a lower microhardness level was observed in the IC HAZ region of the X80 steel. This was due to the lower carbon content in the X80 steel and the formation of the ferrite-bainite microstructure, characterized by predominantly granular morphology, as well as small both retained austenite and twinned martensite proportions. The results of the tensile tests indicated that the viscoplastic characteristics of the X80 welded specimen were preserved (its elongation decreased by 11% only). It could be concluded that decreased carbon contents in steels with their complex microalloying, which results in a dispersed homogeneous ferrite-bainite microstructure, can improve ductility of their laser welded joints.

Upon laser welding of thick plates, the cooling rate of a weld zone will be lower. Respectively, it contributes to the formation of a greater proportion of bainite microstructural components with lower microhardness values. Therefore, laser welding can be considered as a promising method for joining thick parts. Some new results in this area will be given in following papers by the authors.

5. Conclusions

The microstructural studies were carried out of the laser welded joints of the X70 and X80 of low-carbon steels with different initial microstructures, as well as chemical and phase compositions. The X70 steel microstructure was varied by helical rolling at the temperatures of

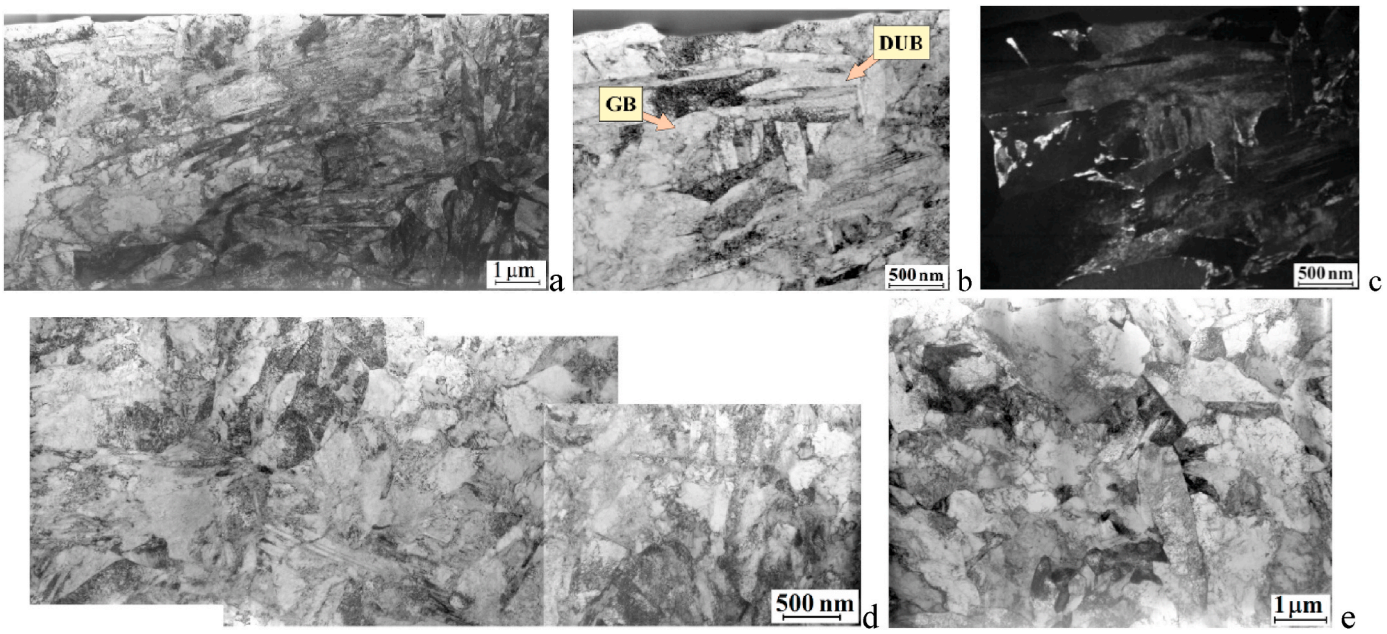

Fig. 8. The TEM-images of the IC HAZ microstructures in the X70-920 (a-c), X70-850 (d) and X80 (e) steels: (a-b, d-e) – bright-field images; c – the dark field images in the reflex from γ-Fe.

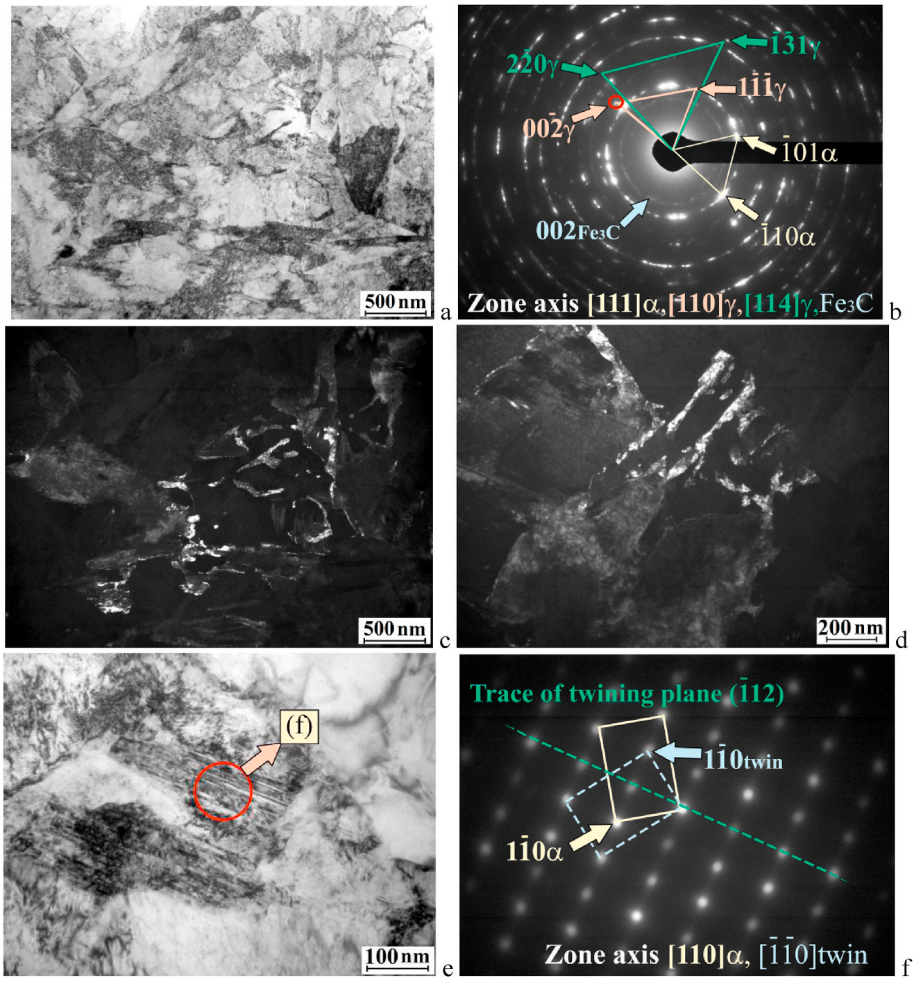

Fig. 9. The TEM-images of the X70-850 IC HAZ: bright-field image in a bainite region (a); microdiffraction pattern with the [111]α, [110]γ zones (b); dark-field images in the $00\bar{2}$ γ reflex (c); dark-field images in the austenite reflex (d); bright-field image in the twinned martensite area (e); the corresponding micro-diffraction pattern (f).

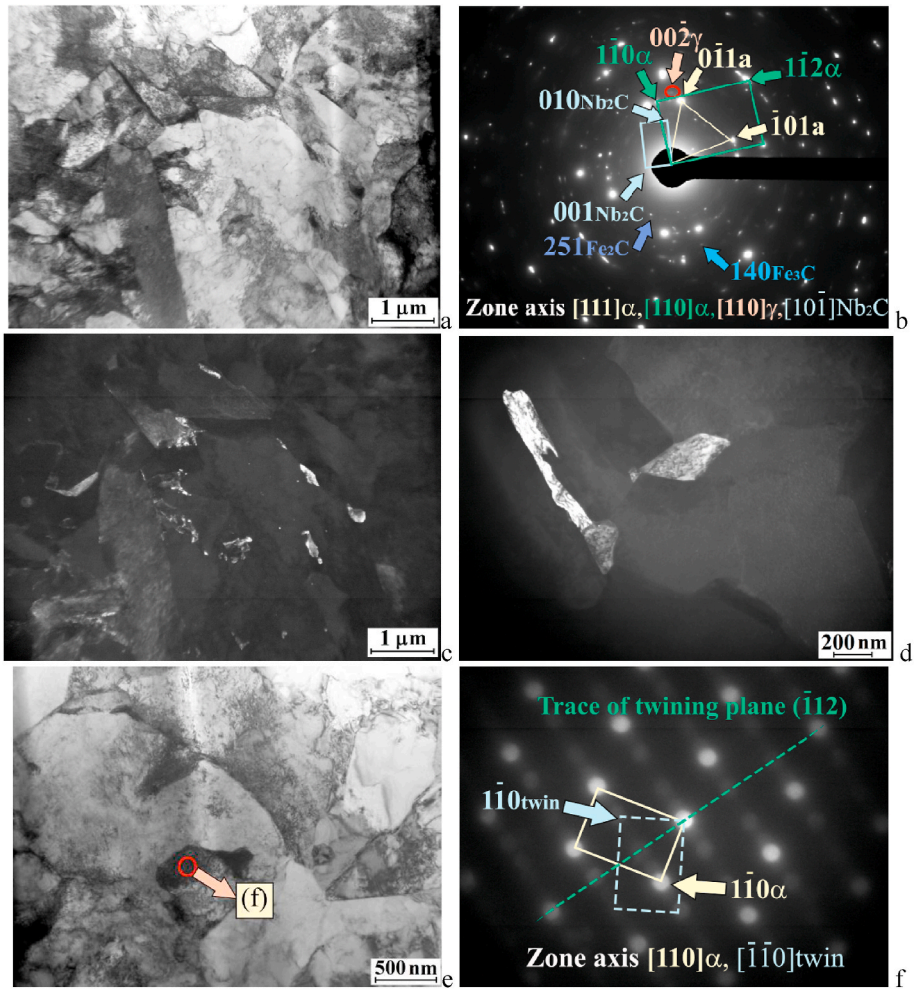

Fig. 10. The TEM images of the X80 IC HAZ microstructure: bright-field images (a and e); microdiffraction pattern showing reflexes of the [111]α, [110]α, [110]γ, [10$\bar{1}$]Nb_2C zones (b); dark-field images in the 00$\bar{2}$ γ reflex (c and d); microdiffraction pattern (f) from the area indicated in Fig. 10, e.

Table 3
Dimensions of the IC HAZ microstructural components.

Steel	Phase[a]	h_B, nm	S_{RA}, nm	V_{RA}, %	$S_{area\ twin}$, nm
X70-920	F + DUB GB (little)	DUB: 50–300 GB: 700–1500	(20–40) × 150-400	9	500—700 ×up to 1600
X70-850	F + GB DUB (little)	GB: 500–1500 DUB: 150–300	Small (10–30) × 90–200; Large (40–70) × 600	7	(10–30) × 200 (40–160) × 200–600
X80	F + GB DUB (little)	GB 500–1500 DUB: 60–200	Small (15–40) × 200; Large (40–160) × (500–800)	4	200 × 200, 80 × 600

[a] DUB is degenerate upper bainite; GB is granular bainite; h_B is widths of the bainitic ferrite regions; S_{RA} is dimensions of retained austenite areas; V_{RA} is the retained austenite proportion; $S_{area\ twin}$ is sizes of twinned martensite zones.

920 and 850 °C.

1. It was shown that the microhardness level was lower (340 HV) in the X70-850 weld metal (WM) with the initially more dispersed and homogeneous ferrite-bainite-pearlite microstructure (d_F = 3.3 μm) compared to the X70-920 one (d_F = 5.5 μm, 370 HV). This reason was the formation of the less stressed microstructure that included lath bainite along with martensite.
2. The microhardness values reduced down to 295 HV in the WM of the X80 steel possessing the lower carbon content (0.055% C) but including chromium, molybdenum and nickel as additional micro-alloying elements, as well as characterized by the initial predominantly ferrite-bainite microstructure (d_F = 4 μm). This was due to the degenerate upper bainite formation and the reduced carbon content in martensite.
3. The results of the IC HAZ studies showed that degenerate upper bainite had formed with the highest retained austenite proportion of 9% and large twinned martensite areas in the X70-920 steel. On the contrary, the granular ferrite-bainite microstructures with the lower retained austenite proportions and the smaller dimensions of twinned martensite regions were found in the X70-850 and X80 ones.

Table 4
The results of the tensile tests.

Steel	YS, MPa	UTS, MPa	ε, %
X70-920, base metal	440 ± 15	735 ± 20	22 ± 1.5
X70-920, welded sample	480 ± 15 **↑9%**	690 ± 15 **↓6%**	16 ± 1.5 **↓27%**
X70-850, base metal	490 ± 15	780 ± 15	20.5 ± 1.5
X70-850, welded sample	570 ± 15 **↑16%**	755 ± 15 **↓3%**	15 ± 1.5 **↓26%**
X80, base metal	550 ± 10	680 ± 10	18.0 ± 1
X80, welded sample	550 ± 10	670 ± 10	16 ± 1 **↓11%**

4. The ultimate tensile strength characteristics of the welded samples decrease slightly (by 3–6%) for both steels. However, ductility of the X70 welded specimens reduced by about 25%, while it lowered by 11% only for the X80 one.
5. It was concluded that using of steels, characterized by dispersed homogeneous ferrite-bainite microstructures due to complex microalloying, reduced carbon contents and thermomechanical treatment, enables to solve the issue of improving ductility of their laser welded joints.

Data availability

The raw/processed data required to reproduce these findings cannot be shared at this time as the data also forms part of an ongoing study.

CRediT authorship contribution statement

A.I. Gordienko: Conceptualization, Methodology, Writing – original draft, Writing – review & editing. **A.G. Malikov:** Methodology, Investigation, Resources. **M.N. Volochaev:** Investigation, Visualization, Validation. **A.D. Panyukhina:** Investigation, Validation.

Declaration of competing interest

The authors declare that they have no known competing financial interests or personal relationships that could have appeared to influence the work reported in this paper.

Acknowledgments

Microstructural studies and mechanical tests of laser welds were performed according to the Government research assignment for ISPMS SB RAS, project FWRW-2021-0009. Part of the research related to the selection of optimal laser welding parameters for low carbon steels was carried out within Basic State Project No. 121030900259-0.

TEM studies were carried out in Center of Federal Research Center of Kirensky Institute of Physics SB RAS. The authors are grateful to I.P. Mishin for assistance in cross-helical rolling of the steel and Mikhail Slobodyan for translation into English.

References

[1] J.C.F. Jorge, J.L.D. Monteiro, A.J.D.C. Gomes, I.D.S. Bott, L.F.G. De Souza, M. C. Mendes, L.S. Araújo, Influence of welding procedure and PWHT on HSLA steel weld metals, J. Mater. Res. Technol. 8 (2019) 561–571, https://doi.org/10.1016/j.jmrt.2018.05.007.

[2] A. de Sousa Lins, L.F.G. de Souza, M.C. Fonseca, Characterization of mechanical properties and residual stress in API 5L X80 steel welded joints, J. Mater. Eng. Perform. 27 (2018) 124–137, https://doi.org/10.1007/s11665-017-3090-z.

[3] D. Kong, C. Ye, W. Guo, Y. Wu, D. Long, Microstructures and plane energy spectra of X80 pipeline steel welded joints by submerged arc automatic welding, J. Wuhan Univ. Technol.-Materials Sci. Ed. 29 (2014) 1265–1269, https://doi.org/10.1007/s11595-014-1079-0.

[4] E.M. Shamov, N.N. Evtiheev, I.N. Shiganov, I.A. Begunov, Technology and equipment for laser welding of annular pipes junction in fixed position of gas-main pipelines, J. Phys. Conf. Ser. 1109 (2018), https://doi.org/10.1088/1742-6596/1109/1/012025.

[5] H. Mostaan, P. Saeedpour, H. Ahmadi, A. Nouri, Laser welding of dual-phase steels with different silicon contents: phase evolutions, microstructural observations, mechanical properties, and fracture behavior, Mater. Sci. Eng. 811 (2021), https://doi.org/10.1016/j.msea.2021.140974, 140974.

[6] X.N. Wang, C.J. Chen, H.S. Wang, S.H. Zhang, M. Zhang, X. Luo, Microstructure formation and precipitation in laser welding of microalloyed C-Mn steel, J. Mater. Process. Technol. 226 (2015) 106–114, https://doi.org/10.1016/j.jmatprotec.2015.07.010.

[7] J. Wang, L. Yang, M. Sun, T. Liu, H. Li, Effect of energy input on the microstructure and properties of butt joints in DP1000 steel laser welding, Mater. Des. 90 (2016) 642–649, https://doi.org/10.1016/j.matdes.2015.11.006.

[8] Q. Jia, W. Guo, W. Li, P. Peng, Y. Zhu, G. Zou, Y. Peng, Z. Tian, Experimental and numerical study on local mechanical properties and failure analysis of laser welded DP980 steels, Mater. Sci. Eng. 680 (2017) 378–387, https://doi.org/10.1016/j.msea.2016.10.121.

[9] L.S. Derevyagina, A.I. Gordienko, Orishich, A.G. Malikov, N.S. Surikova, M. N. Volochaev, Microstructure of intercritical heat affected zone and toughness of microalloyed steel laser welds, Mater. Sci. Eng. 770 (2020) 138522, https://doi.org/10.1016/j.msea.2019.138522.

[10] X.N. Wang, Q. Sun, Z. Zheng, H.S. Di, Microstructure and fracture behavior of laser welded joints of DP steels with different heat inputs, Mater. Sci. Eng. 699 (2017) 18–25, https://doi.org/10.1016/j.msea.2017.05.078.

[11] M. Mandal, W. Poole, M. Militzer, L. Collins, Mechanical properties of intercritically annealed X80 line pipe steels, Metall. Mater. Trans. A Phys. Metall. Mater. Sci. 52 (2021) 1336–1352, https://doi.org/10.1007/s11661-021-06152-5.

[12] J. Wang, P.J. Van Der Wolk, S. Van Der Zwaag, On the influence of alloying elements on the bainite reaction in low alloy steels during continuous cooling, J. Mater. Sci. 35 (2000) 4393–4404, https://doi.org/10.1023/A:1004865209116.

[13] A.A. Kruglova, V.V. Orlov, E.I. Khlusova, Effect of hot plastic deformation in the austenite interval on structure formation in low-alloyed low-carbon steel, Met. Sci. Heat Treat. 49 (2007) 556–560, https://doi.org/10.1007/s11041-007-0102-x.

[14] X. wei Chen, G. ying Qiao, X. lin Han, X. Wang, F. ren Xiao, B. Liao, Effects of Mo, Cr and Nb on microstructure and mechanical properties of heat affected zone for Nb-bearing X80 pipeline steels, Mater. Des. 53 (2014) 888–901, https://doi.org/10.1016/j.matdes.2013.07.037.

[15] Y. You, C. Shang, S. Subramanian, Effect of Ni addition on toughness and microstructure evolution in coarse grain heat affected zone, Met. Mater. Int. 20 (2014) 659–668, https://doi.org/10.1007/s12540-014-4011-4.

[16] S.M. Hasan, S. Kumar, D. Chakrabarti, S.B. Singh, Effect of prior austenite grain size on the formation of carbide-free bainite in low-alloy steel, Philos. Mag. A 100 (2020) 2320–2334, https://doi.org/10.1080/14786435.2020.1764653.

[17] C. Celada-Casero, J. Sietsma, M.J. Santofimia, The role of the austenite grain size in the martensitic transformation in low carbon steels, Mater. Des. 167 (2019), https://doi.org/10.1016/j.matdes.2019.107625.

[18] T. Hanamura, S. Torizuka, S. Tamura, S. Enokida, H. Takech, Effect of austenite grain size on the mechanical properties in air-cooled 0.1c-5Mn martensitic steel, Mater. Sci. Forum (2014) 783–786. https://doi.org/10.4028/www.scientific.net/msf.783-786.1027, 1027–1032.

[19] A. García-Junceda, C. Capdevila, F.G. Caballero, C.G. de Andrés, Dependence of martensite start temperature on fine austenite grain size, Scripta Mater. 58 (2008) 134–137, https://doi.org/10.1016/j.scriptamat.2007.09.017.

[20] J. Hidalgo, M.J. Santofimia, Effect of prior austenite grain size refinement by thermal cycling on the microstructural features of as-quenched lath martensite, Metall. Mater. Trans. A Phys. Metall. Mater. Sci. 47 (2016) 5288–5301, https://doi.org/10.1007/s11661-016-3525-4.

[21] A. Sabet Ghorabaei, M. Nili-Ahmadabadi, Effects of prior austenite grain size and phase transformation temperature on bainitic ferrite formation in multi-constituent microstructures of a strong ultra-low-carbon steel, Mater. Sci. Eng. 815 (2021) 141300, https://doi.org/10.1016/j.msea.2021.141300.

[22] H.S. Yang, H.K.D.H. Bhadeshia, Austenite grain size and the martensite-start temperature, Scripta Mater. 60 (2009) 493–495, https://doi.org/10.1016/j.scriptamat.2008.11.043.

[23] X. Liang, A.J. Deardo, A study of the influence of thermomechanical controlled processing on the microstructure of bainite in high strength plate steel, Metall. Mater. Trans. A Phys. Metall. Mater. Sci. 45 (2014) 5173–5184, https://doi.org/10.1007/s11661-014-2444-5.

[24] L. Lan, Z. Chang, X. Kong, C. Qiu, D. Zhao, Phase transformation, microstructure, and mechanical properties of X100 pipeline steels based on TMCP and HTP concepts, J. Mater. Sci. 52 (2017) 1661–1678, https://doi.org/10.1007/s10853-016-0459-6.

[25] M. Eroglu, M. Aksoy, Effect of initial grain size on microstructure and toughness of intercritical heat-affected zone of a low carbon steel, Mater. Sci. Eng. 286 (2000) 289–297, https://doi.org/10.1016/S0921-5093(00)00801-7.

[26] T. Lolla, S.S. Babu, S. Lalam, M. Manohar, Understanding the role of initial microstructure on intercritically reheated heat-affected zone microstructures and properties of microalloyed steels, in: ASM Proc. Int. Conf. Trends Weld, . Res., 2013, pp. 34–42.

[27] O.M. Akselsen, Grong, J.K. Solberg, Structure-property relationships in intercritical heat affected zone of low-carbon microalloyed steels, Mater. Sci. Technol. 3 (1987) 649–655, https://doi.org/10.1179/mst.1987.3.8.649.

[28] A.I. Gordienko, L.S. Derevyagina, A.G. Malikov, Orishich, N.S. Surikova, M. N. Volochaev, The effect of the initial microstructure of the X70 low-carbon microalloyed steel on the heat affected zone formation and the mechanical properties of laser welded joints, Mater. Sci. Eng. 797 (2020), https://doi.org/10.1016/j.msea.2020.140075.

[29] L.S. Derevyagina, A.I. Gordienko, N.S. Surikova, M.N. Volochaev, Effect of helical rolling on the bainitic microstructure and impact toughness of the low-carbon microalloyed steel, Mater. Sci. Eng. 816 (2021) 141275, https://doi.org/10.1016/j.msea.2021.141275.

[30] A. Malikov, N. Bulina, M. Sharafutdinov, A. Orishich, Study of the structure and phase composition of laser welded joints of Al-Cu-Li alloy under different heat treatment conditions, Int. J. Adv. Manuf. Technol. 104 (2019) 4313–4324, https://doi.org/10.1007/s00170-019-04286-w.

[31] A. Malikov, I. Vitoshkin, A. Orishich, A. Filippov, E. Karpov, Microstructure and mechanical properties of laser welded joints of Al-Cu-Li and Ti-Al-V alloys, J. Manuf. Process. 53 (2020) 201–212, https://doi.org/10.1016/J.JMAPRO.2020.02.010.

[32] Y. Shao, C. Liu, Z. Yan, H. Li, Y. Liu, Formation mechanism and control methods of acicular ferrite in HSLA steels: a review, J. Mater. Sci. Technol. 34 (2018), https://doi.org/10.1016/j.jmst.2017.11.020.

[33] S.M.C. van Bohemen, L. Morsdorf, Predicting the Ms temperature of steels with a thermodynamic based model including the effect of the prior austenite grain size, Acta Mater. 125 (2017) 401–415, https://doi.org/10.1016/J.ACTAMAT.2016.12.029.
[34] P. Kirkwood, Enhancing the weldability of C-Mn pressure vessel steels — a tale of two elements, Energy Mater. (2014) 61–70, https://doi.org/10.1007/978-3-319-48765-6_7.
[35] C. Heinze, A. Pittner, M. Rethmeier, S.S. Babu, Dependency of martensite start temperature on prior austenite grain size and its influence on welding-induced residual stresses, Comput. Mater. Sci. 69 (2013) 251–260, https://doi.org/10.1016/j.commatsci.2012.11.058.
[36] J. Calvo, I.H. Jung, A.M. Elwazri, D. Bai, S. Yue, Influence of the chemical composition on transformation behaviour of low carbon microalloyed steels, Mater. Sci. Eng. 520 (2009) 90–96, https://doi.org/10.1016/j.msea.2009.05.027.
[37] Offshore Standard DNV-OS-F101 «Submarine Pipeline Systems», 2012.
[38] M. Olasolo, P. Uranga, J.M. Rodriguez-Ibabe, B. López, Effect of austenite microstructure and cooling rate on transformation characteristics in a low carbon Nb-V microalloyed steel, Mater. Sci. Eng. 528 (2011) 2559–2569, https://doi.org/10.1016/j.msea.2010.11.078.